# Morphological Analysis of Retinal Microvasculature to Improve Understanding of Retinal Hemorrhage Mechanics in Infants

Matt P. Byrne, Kendall R. McMillan, and Brittany Coats

Department of Mechanical Engineering, University of Utah, Salt Lake City, Utah, United States

Correspondence: Brittany Coats, 1495 E 100 S, 1550 MEK, Salt Lake City, UT 84112, USA; brittany.coats@utah.edu.

**Received:** July 11, 2019
**Accepted:** December 31, 2019
**Published:** March 16, 2020

Citation: Byrne MP, McMillan KR, Coats B. Morphological analysis of retinal microvasculature to improve understanding of retinal hemorrhage mechanics in infants. *Invest Ophthalmol Vis Sci.* 2020;61(3):16. https://doi.org/10.1167/iovs.61.3.16

**Purpose.** In this experimental study, we quantify retinal microvasculature morphological features with depth, region, and age in immature and mature ovine eyes. These data identify morphological vulnerabilities in young eyes to inform the mechanics of retinal hemorrhage in children.

**Methods.** Retinal specimens from the equator and posterior pole of preterm (n = 4) and adult (n = 9) sheep were imaged using confocal microscopy. Vessel segment length, diameter, angular asymmetry, tortuosity, and branch points were quantified using a custom image segmentation code. Significant differences were identified through two-way ANOVAs and correlation analyses.

**Results.** Vessel segment lengths were significantly shorter in immature eyes compared to adults ($P < 0.003$) and were significantly shorter at increasing depths in the immature retina ($P < 0.04$). Tortuosity significantly increased with depth, regardless of age ($P < 0.05$). These data suggest a potential vulnerability of vasculature in the deeper retinal layers, particularly in immature eyes. Preterm retina had significantly more branch points than adult retina in both the posterior pole and equator, and the number increased significantly with depth ($P < 0.001$).

**Conclusions.** The increased branch points and decreased segment lengths in immature microvasculature suggest that infants will experience greater stress and strain during traumatic loading compared to adults. The increased morphological vulnerability of the immature microvasculature in the deeper layers of the retina suggest that intraretinal hemorrhages have a greater likelihood of occurring from trauma compared to preretinal hemorrhages. The morphological features captured in this study lay the foundation to explore the mechanics of retinal hemorrhage in infants and identify vulnerabilities that explain patterns of retinal hemorrhage in infants.

Keywords: ocular trauma, retinal hemorrhage, pediatrics, mechanics

Discerning between abusive and accidental trauma in children is of critical importance to the pediatrician, as diagnosing abuse early may affect the survival of the young patient. Retinal hemorrhage (RH) is reported to varying extents in 50% to 100% of abusive head trauma (AHT) cases.[1–5] However, few data exist on the mechanics of RH or the forces required to create these hemorrhages in young children and infants. Understanding the failure of structures begins with an understanding of the microstructural features that influence the mechanical response of the structure. In the case of RH, the microvascular morphology, such as the number of branch points, vessel segment length, and vessel diameter, will contribute to the behavior of the retinal vascular network as a whole. Therefore, an understanding of the morphology of the microvasculature is needed to identify factors that may contribute to the failure of the vessel walls during trauma and lead to RH.

Morphological characterization of large retinal vessels is reported in the literature,[6–9] but these studies focus on the method of morphology characterization or the morphology related to pathologies such as Parkinson's disease in adults. Studies specific to children and adolescents used two-dimensional (2D) fundus images to characterize the optic disc and major retinal blood vessel characteristics in normal[7] or hypertensive[10] patients. Most traumatic RH in children is intraretinal,[11,12] which suggests injury is more likely associated with microvasculature structure and cannot be captured in detail with fundus imaging. Some descriptive studies have evaluated retinal vascular morphology through the depth of the retina in adolescents and adults,[13–15] but very little quantitative characterization was performed. Furthermore, no studies have evaluated changes in retinal vascular morphology with age.

The objective of this study was to quantify changes in the morphological features of retinal microvasculature with retinal depth and age to inform the mechanics of potential RH and to identify morphological vulnerabilities in younger eyes. Understandably, obtaining human infant eyes for evaluation is challenging; therefore, comparisons of age-related trends are often found in non-human species to provide






Investigative Ophthalmology & Visual Science

Table. Microscopy Images Collected by Specimen ID, Age of Specimen, and Thickness of the Image Stack as Measured from the Inner Limiting Membrane

| Specimen ID | Age | Depth from ILM (μm) Equatorial; Posterior |
|---|---|---|
| Ad-1 | 6 y | 95.15; — |
| Ad-2 | 6 y | 157.73; 172.80 |
| Ad-3 | 6 y | 153.15; 182.20 |
| Ad-4 | 6 y | 133.40; 132.15 |
| Ad-5 | 6 y | 119.05; 117.20 |
| Ad-6 | 6 y | 129.65; 123.35 |
| Ad-7 | 6 y | 48.10; 103.48 |
| Ad-8 | 6 y | 163.35; 112.48 |
| Ad-9 | 6 y | 117.90; 67.68 |
| Pre-1 | 132 d gestation | 78.18; 116.73 |
| Pre-2 | 132 d gestation | 138.20; 123.15 |
| Pre-3 | 131 d gestation | 88.20; 108.48 |
| Pre-4 | 131 d gestation | —; 98.87 |

insight into human trends. This approach has been found to be successful in understanding age-related changes in the mechanics of brain tissue, vitreous, and other biological materials.[16,17] For this study, we selected sheep as the non-human model to evaluate age- and region-related changes in retinal vasculature. Sheep have a holangiotic vascular pattern like humans and a well-defined retinal structure. They also exhibit similar regional trends in vitreoretinal adhesion compared to human eyes.[18] When selecting an animal model, it is important to consider how the ages of the model compare to the developmental stages in humans. Based on reproductive maturity and life span, adult sheep 5 to 6 years old are roughly equivalent to humans 28 to 36 years of age. Using neurological development patterns, we estimate that preterm lambs (131–132 days gestational age) are equivalent to humans 6 to 12 months old.[19] Therefore, the use of these data will be most valuable in identifying age-specific vasculature characteristics between infants and adults and will provide insight into age-dependent morphological features that may result in higher risks of RH from trauma.

## Methods

### Specimen Preparation

All studies were reviewed by the University of Utah Institutional Review Board and Institutional Animal Care and Use Committee and adhere to the Association for Research in Vision and Ophthalmology Statement for the Use of Animals in Ophthalmic and Vision Research. The eyes used in this study were sourced from existing non-ocular studies at the University of Utah. Eyes obtained from adult ewes 5 to 6 years old (n = 9) and preterm lambs delivered by caesarian section at 131 to 132 days gestation (n = 4) were enucleated en bloc, then immediately fixed whole with 4% paraformaldehyde. The axial and transverse lengths of the preterm eyes were approximately 19 mm and 22.5 mm, respectively. The axial and transverse lengths of the adult eyes were approximately 31 mm and 34.5 mm, respectively. After overnight fixation at 4°C, extraocular fatty tissue and muscles were trimmed away from the eye. An 8-mm tissue punch (RS-6330-8; Roboz Surgical Instrument Co., Gaithersburg, MD, USA) was used to extract posterior pole and equatorial retina specimens. This punch represented approximately 2% of the adult sheep retina and 5% of the preterm sheep retina. The sheep tapetum is located in the choroid and therefore was not included in the specimen. The Table summarizes the subjects, their relative ages, the regions sampled, and the imaging depths. The depths were defined in relation to the approximate location of the inner limiting membrane (ILM). For reference, adult ovine retinal thickness is around 250 μm near the optic nerve and tapers to 100 μm near the periphery.[20] In a previous study conducted by our group, we found no significant difference between adult and preterm ovine retinal thickness (179 ± 36 μm vs. 182 ± 45 μm for adult and preterm, respectively).[21]

After the retinal specimens were successfully removed from the eye, they were placed overnight at 4°C into a block buffer solution containing 5% bovine serum albumin (A9418; Sigma-Aldrich, St. Louis, MO, USA) and 0.5 % Triton X-100 lysis buffer (BP-117X; Boston BioProducts, Ashland, MD, USA) in PBS. The specimens were washed with PBlec (BM-733; Boston BioProducts). Isolectin GS-IB4 from *Griffonia simplicifolia*, Alexa Fluor 488 conjugate was used for labeling (A10235; Invitrogen, Carlsbad, CA, USA). The conjugate was diluted to 1:100 in PBlec, added to each specimen, and incubated overnight at 4°C. Labeled specimens were washed with PBS and imaged on an A1R+ confocal microscopy system (Nikon Instruments, Melville, NY, USA) beginning at the approximate location of the ILM and increasing in depth toward the retinal pigment epithelium (Fig. 1).[22] The confocal microscope imaged vessels up to a maximum depth of 125 μm from the ILM.

### Morphological Analysis

The confocal microscopy process resulted in a stack of images, each representing a horizontal 2D slice of the retinal vasculature. The penetration depth varied from sample to sample depending on the quality of the staining and thickness of the retina; therefore, we specified three depth ranges that were applicable to all specimens: 6 to 45.67 μm, 45.67 to 85.33 μm, and 85.33 to 125 μm. These depth ranges represent the shallow, mid, and deep sections of the retinal micro vasculature. A representative example of the confocal images obtained for preterm and adult specimens at each depth range is shown in Figure 2.

Six morphological features were evaluated: vessel segment length, vessel segment diameter, vessel segment

Investigative Ophthalmology & Visual Science

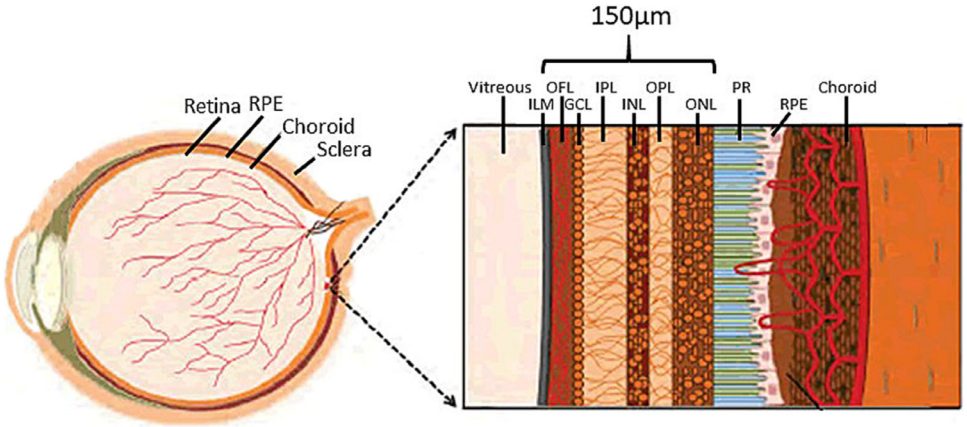


**Figure 1.** A schematic of the layers of the sheep retina at the posterior pole. GCL, ganglion cell layer; ILM, inner limiting membrane; INL, inner nuclear layer; IPL, inner plexiform layer; OFL, optic fiber layer; ONL, outer nuclear layer; OPL, outer plexiform layer; PR, photoreceptor; RPE, retinal pigment epithelium. Image modified from Nowak-Sliwinska et al.,[22] licensed under CC BY 4.0.

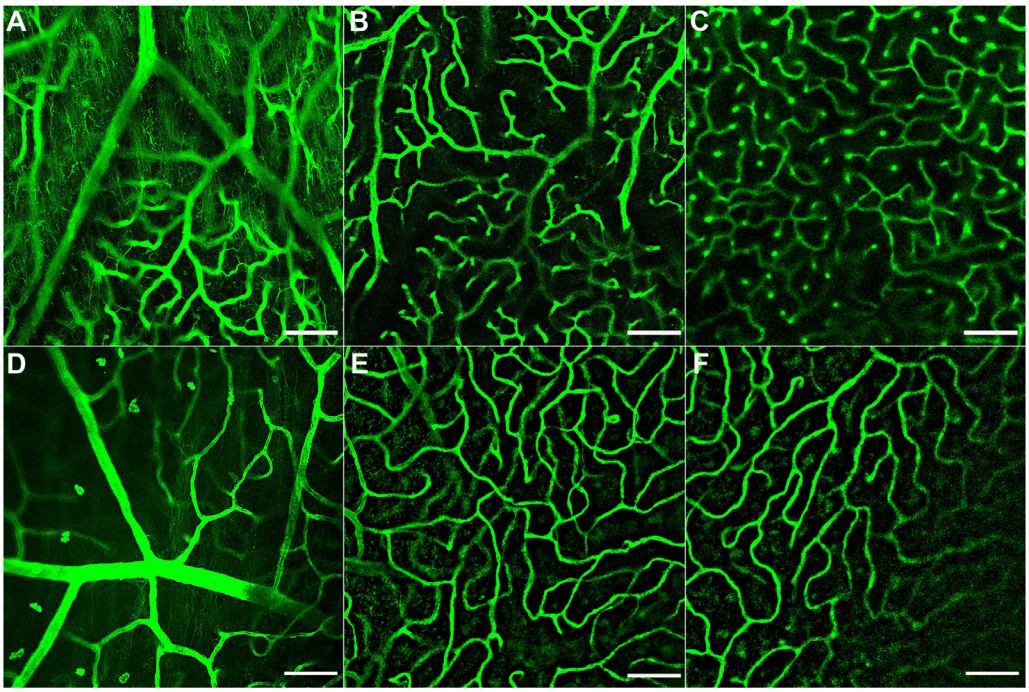


**Figure 2.** Examples of retinal vasculature in preterm (**A–C**) and adult (**D–F**) eyes. Images represent the shallow (**A**, **D**), mid (**B**, **E**), and deep (**C**, **F**) sections of analysis. *Scale bar*: 100 µm.

length-to-diameter ratio, angular asymmetry, tortuosity, and number of branch points. These morphological features were selected because they have been used to characterize blood vessel morphology in other studies and because they all potentially influence the mechanics of blood vessels. For example, a smaller vessel diameter or shorter vessel segment length will result in greater stress and strain, respectively, when loaded the same as a larger vessel diameter or longer vessel segment length. Increased tortuosity may increase the risk of pressure-related damage to a vessel, and an increased number of branch points may provide increased opportunities for failure at these junctions.

To analyze these morphological features in each animal and in each region, three images were selected from each confocal image stack. The three images represented the shallowest image in the stack where vessels could be clearly seen, the deepest image in the stack where vessels could be clearly seen, and then an image from their midpoint. A MATLAB code (MathWorks, Natick, MA, USA; available on GitHub[23]) was created to quantify vessel segment length, diameter, length-to-diameter ratio, angular asymmetry, and tortuosity in each 2D slice. The number of vessel segments and branch points in each 2D image were also quantified. All image analyses were performed by a single observer. A detailed description of each of these morphological features is provided in the following subsections.

**Vessel Segment Length.** The length of a vessel segment was defined as the distance from a terminal point

Investigative Ophthalmology & Visual Science

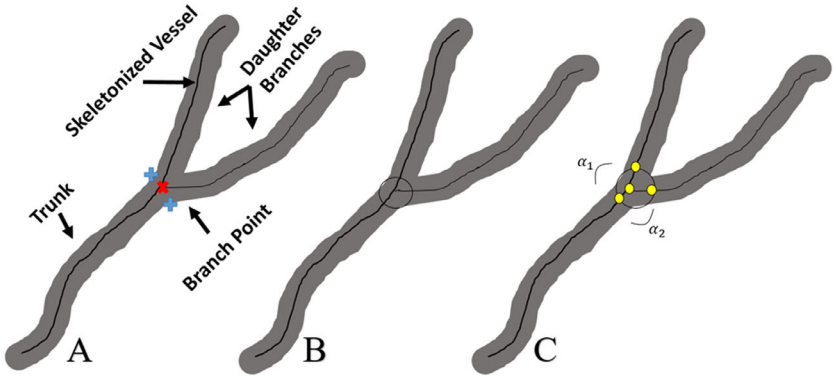


**Figure 3.** (**A**) Schematic of a vessel (gray) with an overlaid skeleton (black). The custom analysis program placed a red marker on the branch point, and a user specified two points representing the diameter at that point (blue). (**B**) A virtual circle using 1/2 the diameter as the radius was created around the branch point. The intersection of the circle with the skeletonized vessel identified the three pixels used to define $\alpha_1$ and $\alpha_2$.

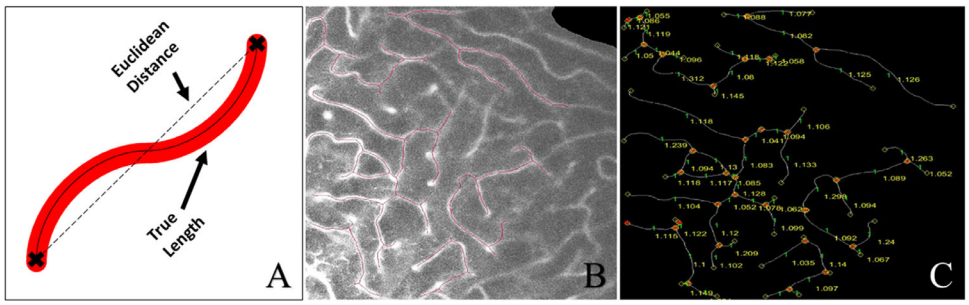


**Figure 4.** (**A**) Tortuosity was defined as the ratio of the true length of the vessel segment (solid black line) and the Euclidean distance (dashed line) between the end points. (**B**) An example of the skeletonized vessel segments (red) overlaid with the image of the vessel network, and (**C**) the associated tortuosity values for each vessel segment.

of a vessel to a branch point or from one branch point to another branch point. This measurement was taken along the midline of the vessel segment using a skeletonization technique and represents the true length of the retinal segment rather than the Euclidean distance between endpoints.

**Vessel Segment Diameter.** To quantify vessel segment diameter, the MATLAB program presented the user with an image containing marks along each quartile of the vessel segment length. The user selected the outer pixels of the vessel at those quartile locations to define each quartile diameter. The three quartile diameter measurements were averaged for a representative vessel segment diameter.

**Angular Asymmetry.** The protocol for measuring angular asymmetry was modified from a previously described method.[6] For each branch point identified in the image, the user manually selected two points representing the outer diameter of the vessel at that branch point (Fig. 3A). The distance between these points was halved to generate the radius of a circle revolving around the branch point (Fig. 3B). Three pixels on the skeletonized vessel intersected the circle and were used to measure the angle of the daughter branches ($\alpha_1$ and $\alpha_2$) with the trunk (Fig. 3C). Angular asymmetry was defined as the absolute difference between the angle of each daughter branch ($\alpha_1$ and $\alpha_2$).

**Tortuosity.** Using the end points and branch points of the skeletonized vessels, tortuosity was calculated by dividing the true segment length by the Euclidean distance between the end points or branch points. Figure 4 illustrates this calculation and provides an example of a skeletonized image with the associated tortuosity of each vessel.

## Data Analysis

The morphological quantities within each 2D image were not normally distributed, so a median value was used to represent the morphological features in each image. The median diameter measurements involved the most user interaction during quantification, so intraobserver repeatability was assessed on this morphological feature using a subset of 10 images. Repeatability was quantified using a correlation coefficient and coefficient of repeatability and visually by using a Bland–Altman plot. To identify significant trends in retinal depth, morphological features were statistically correlated using Pearson's product–moment correlation with exact depth for each region within each age group. Then, two two-way ANOVAs were performed to determine the effect of age and depth on each morphological characteristic for each region, and the effect of the depth and region for each age. For these statistical tests, depth values were stratified as described previously to represent shallow, mid, and deep vessel sections. All statistics were performed using JMP Pro 13.1.0 (SAS Institute, Cary, NC, USA). A type I error of 5% was used to define significance throughout all statistical evaluations.

Investigative Ophthalmology & Visual Science

## Results

### Intraobserver Repeatability

Median diameters from 10 images had an average difference of 0.56 µm with a standard deviation of differences of 0.77 µm. The Pearson correlation coefficient between measurements was 0.93. The coefficient of repeatability was 0.64 µm, which indicates that 95% of repeated measurements will be within 0.64 µm of each other. Given that the magnitudes of the median diameters in the 10 images ranged from 7.2 to 12.7 µm, a 0.64 µm variation in measurement was deemed reasonable. No trends of increasing bias with increasing diameter were identified on the Bland–Altman plot.

### Vessel Segment Length

Preterm vessel segment length significantly decreased as depth increased in the equator ($P = 0.0024$) (Fig. 5A). The trend was also seen in the posterior pole, but it was not significant due to one data point ($P = 0.0714$). If that data point were removed, the significance became $P = 0.0303$. Adult vessel segment lengths did not show a decreasing trend with depth. When analyzing the age and depth effects for each region, the equatorial region was significantly affected by age ($P = 0.0025$) and depth ($P = 0.0242$). Adult vessel segments were significantly longer than preterm vessel segments and were significantly longer in the shallow depth compared to the mid and deep depths. Analysis of the age and depth effects for the posterior pole region indicated that deeper vessel segments (farther from the ILM) were significantly shorter than shallow vessel segments when the ages were combined ($P = 0.0453$). The ANOVA evaluation of the depth and regional effects with each age found that preterm subjects had significantly shorter segment lengths with increasing depth ($P = 0.0366$), confirming our correlation analysis. This was true in both the equator and posterior pole. For adult vasculature, there was a significant effect of region ($P < 0.02$) where equatorial segment lengths were longer than posterior pole segments.

### Diameter

Median vessel segment diameters ranged from 6 to 16 µm, suggesting that most of the measurements were of capillaries in the retina rather than larger vessels. When evaluating continuous depth data, we did not find significant correlations between the diameter of vessels and their depth within the retina for either age; however, when stratified according to shallow, mid, and deep sections, there was a significant depth effect in the posterior pole ($P = 0.0207$). Specifically, the diameters of blood vessels in the deeper layers of the retina in both ages were significantly smaller than the shallow and mid-range blood vessel diameters. We did not find a significant age effect on diameter. However, we observed that vessels in the preterm posterior pole generally had a smaller diameter deeper into the retina. This observation was not statistically significant ($P = 0.0745$) (Fig. 5B). There were no significant region effects.

### Length-to-Diameter Ratio

We did not see any significant correlations between the length-to-diameter ratio of blood vessels and their depth within the retina (Fig. 5C). The preterm vessels in the equatorial region generally had lower length-to-diameter ratios deeper into the retina, but this was not a statistically significant trend ($P = 0.0999$). As we looked at the age and depth effects for each region, we found a significant age effect in the equatorial region ($P = 0.0017$). Specifically, the preterm length-to-diameter ratios were significantly lower than the ratios in the adult retina. There were no significant posterior pole effects. When we analyzed depth and regional effects for each age, we did not see any depth and regional effects for preterm retina; however, the equator had significantly higher length-to-diameter ratios than the posterior pole in adult retina ($P = 0.0096$).

### Angular Asymmetry

There was significantly less angular asymmetry in adult posterior pole branches in deeper layers ($P = 0.0228$) (Fig. 5D). This trend was also found in the adult equatorial region, but it was not significant. Preterm posterior pole and equatorial branch asymmetry were significantly less in deeper layers ($P = 0.04$). Neither of the ANOVAs showed any statistically significant effects of age, region, or depth.

### Tortuosity

Tortuosity of blood vessels in the adult equator significantly increased with depth ($P = 0.028$). The adult posterior pole did not demonstrate this trend. There was no significant tortuosity change with increasing retinal depth for the preterm eyes for either region. As we looked at age and depth effects for each region using an ANOVA, we found that there were no significant effects in the equatorial regions; however, the posterior pole had a significant effect with depth ($P = 0.0431$) (Fig. 5E). Specifically, tortuosity of blood vessels when both ages were combined was significantly higher in the deeper layers of the posterior pole retina than the shallow layers. Depth and regional analysis for each age yielded no significant effects on preterm vessel tortuosity, but we found a significant effect of depth in adult specimens ($P = 0.0353$). Blood vessel tortuosity in adult eyes was significantly higher in deeper layers compared to shallow layers when regional data were combined.

### Number of Branches

There were no significant correlations with depth (Fig. 5F); however, when depth was stratified into shallow, mid, or deep, then age, depth, and their interaction all significantly affected the number of branch points in the equator ($P < 0.01$) but not the posterior pole. Specifically, preterm equatorial retina had significantly more branch points than adult equatorial retina ($P < 0.0001$), and there were significantly more branch points in mid and deep layers when compared to shallow layers ($P < 0.0003$). There was also a significant interaction between age and depth for each region as well ($P < 0.0064$). In the posterior pole, preterm eyes generally had more branch points, but this was not significant ($P = 0.0739$).

## Discussion

The goal of this study was to determine whether differences exist in microvascular morphology with age that may predispose infant populations to retinal hemorrhage and,

Investigative Ophthalmology & Visual Science

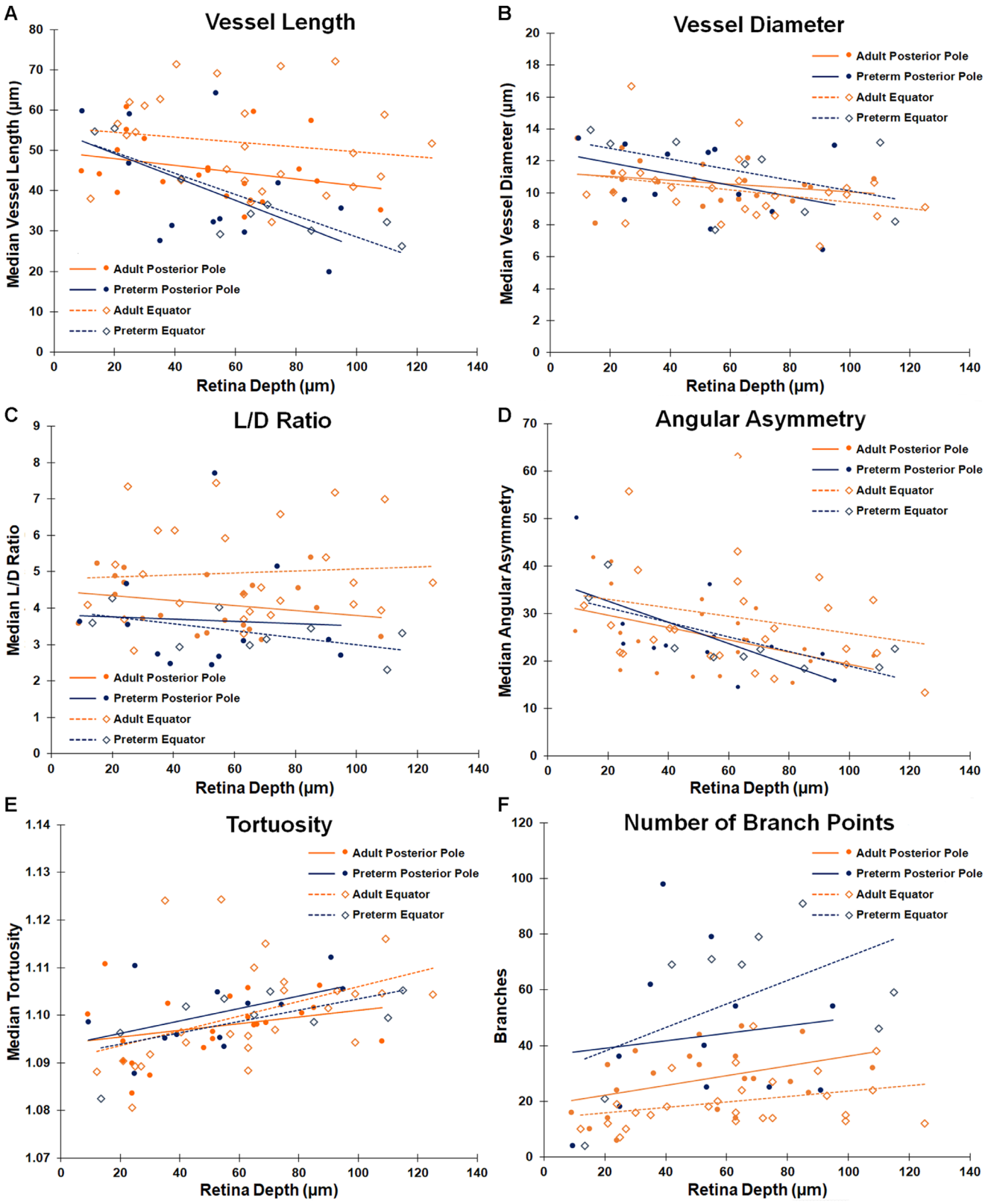


**Figure 5.** Morphological characterization of retinal vessels in preterm (blue) and adult (orange) specimens as a function of depth. (**A**) Preterm vessel segments were significantly shorter than adult segments at all depths and regions and significantly decreased with depth ($P < 0.04$). (**B**) There was no significant correlation between vessel segment diameter and depth for either age or region. When adult and preterm specimens were grouped, posterior pole vessel diameters significantly decreased with depth ($P = 0.02$). (**C**) Preterm equatorial vessels had significantly lower length-to-diameter (L/D) ratios than adult equatorial vessels ($P < 0.002$). The equator had significantly higher

Investigative Ophthalmology & Visual Science

L/D ratios than the posterior pole ($P < 0.01$) in adult retina. (**D**) Angular asymmetry decreased in the adult posterior pole at increasing depths ($P = 0.03$). Preterm asymmetry also significantly decreased at increasing depths in both regions ($P = 0.04$). (**E**) Tortuosity of vessels in the adult equator increased with depth ($P = 0.03$). There were no significant tortuosity changes with depth for preterm eyes in either region, but tortuosity in the posterior pole was significantly greater in deeper layers when both age groups were combined ($P = 0.04$). (**F**) Preterm vessels have significantly more branch points than adult retinal vessels ($P < 0.0001$) at all depths.

if so, whether this is exacerbated in specific regions or depths. We found key morphological characteristics of retinal microvasculature that were different between preterm and adult sheep that would alter the structural strength of the vessels. These differences presented to differing degrees at different depth levels and offer insight into prevalent patterns of RH in abusive head trauma.

## Vessel Segment Lengths are Shorter in Pediatric Retina

The median lengths of preterm retinal blood vessels in the posterior pole and equatorial regions were shorter at all measured depths than the adult vessels. This is not surprising given the growth and maturation process of the retinal vasculature. During development, angiogenesis creates many small vessel segments. As the eye matures, pruning and remodeling occur as the metabolic demand of the retina changes. It is possible that there is some vasculature stretch with retinal growth, but such stretching would likely be accompanied by a reduction in diameter. We found no significant difference in vessel diameters with age; therefore, we believe the changes in vessel structure are primarily due to their own growth and remodeling rather than vessel stretching. In mechanics, injury or failure is defined by stress or strain. Normal stress is defined by an applied force divided by the area on which it acts. Normal strain is a change in length divided by the original length; thus, the shorter vessel segment lengths in the preterm retinal microvasculature will have a propensity for increased strain and increased risk for RH compared to the adult, especially in the deeper layers of the retina where the segments are shortest.

## Microvasculature Diameter, Angular Asymmetry, and Tortuosity are Independent of Age and Region

There was no significant difference between the diameters of equatorial and posterior pole vessels in either the preterm or adult datasets. This was surprising, as we expected vessel diameters to decrease toward the periphery of the retina similar to the changing structure of a tree with thinner branches extending away from the relatively thick trunk. This structure has been described in the literature by Anand-Apte and Hollyfield,[24] but their observation was in reference to larger vessels visible from fundus imaging. Our confocal microscopy captured microvasculature and may represent the smallest denomination of vasculature. When ages were combined, vessel diameter in the posterior pole was significantly reduced in deeper layers of the retina. Mechanical stress will be greater in vessel networks with smaller vessel diameters, which suggests that deeper vessels in the posterior pole of both ages may be more susceptible to higher levels of stress during traumatic loading.

When designing the study, we speculated that large angular asymmetry may provide a greater opportunity for uneven loading at a branch point and for the manifestation of shearing forces, thereby increasing the likelihood of vessel rupture. We found no significant age or region effects with angular asymmetry, but we did find a significant decrease of angular asymmetry with depth. We are not aware of any studies that have investigated how varying angular asymmetry would affect stress in vasculature. Monson et al.[25] reported that branched cerebral vessels experience larger stresses and strains compared to non-branched segments, but they did not evaluate varying branch angles or angular asymmetry. More studies are necessary to understand how specific loading patterns on branched vessels affect stress at the branch sites.

Tortuosity increased with increasing depth within the retina, but this was only significant in the adult equatorial region. An increase in tortuosity suggests an increase in transmural pressure of the vessel[26,27] and potentially an increase in risk of RH. Because blood vessels have critical pressures at which they will buckle and become tortuous,[28] increased tortuosity is generally indicative of increased pressure. However, tortuosity is also dependent on the axial stretch and structural integrity of the blood vessel, so these characteristics would also have to be evaluated to make a true comparison between blood vessels. Regardless, given the ease of visualizing tortuosity in the eye, this metric could have potential to be a metric for the risk of RH, similar to its use in evaluating the risk of retinal detachment in retinopathy of prematurity. The vessel networks imaged in our study were not pressurized and do not give a complete picture of how tortuosity may present in these age groups in vivo. More work is needed to truly evaluate how tortuosity varies between infant and adult eyes and to develop this aspect into a biomarker for risk of RH.

## Infant Eyes have More Branch Points Compared to Adults

There were more branch points in the posterior pole and equatorial regions of the preterm retinas compared to the adult retinas. This was the case for all imaged depths. Similar to the short vessel segment lengths of preterm vasculature, the greater degree of vessel branching in the preterm specimens likely corresponds to the neovascularization that occurs during development and growth of the retina. Neovascularization would be observed as new vessels sprouting from parent vessels, resulting in more branches. Branching has been previously shown to significantly increase the risk of failure in blood vessels under loading.[29–32] Specifically, vessel segments with branches have increased stress and strain compared to unbranched vessel segments, and they rupture at lower intraluminal pressures. Therefore, infants would have an increased risk for RH compared to adults due to the higher number of branch points in the young vessel network. This increased risk would be most prevalent in the deeper layers of the retinal vasculature where branch points are even greater.

Investigative Ophthalmology & Visual Science

### Comparison of Retinal Vasculature Morphology to Clinical Patterns of RH in Infants

In this study, we report certain features of the immature retinal vasculature that make it more vulnerable to injury compared to the adult. These features are the increased branch points and decreased vessel segment length. These two parameters increased vulnerability in deeper layers of the retina compared to superficial layers. In addition, although there was no age-related difference in diameter, decreasing diameter with depth also suggests higher risk for mechanical stress in the deeper layers of the retina. In whole, these data suggest that RH in infants will occur more readily in the mid and deep layers of the retina. This interpretation agrees with patterns of RH reported in the literature. Binenbaum et al.[11] reported that 100% of the children examined in their study of abusive or accidental RH had intraretinal hemorrhages, and 75% of these children had preretinal hemorrhage in addition to the intraretinal hemorrhage. Intraretinal hemorrhages in the study were often too numerous to count, and preretinal hemorrhages, when present, were less numerous. These clinical data suggest that RH occurs more readily in the mid and deep retinal layers rather than superficially. This observation is also in agreement with a large meta-analysis performed by Maguire et al.[12] that reports a far greater incidence of intraretinal hemorrhage compared to preretinal or subretinal hemorrhage.

Another common finding in clinical studies is that RH tends to present in the posterior pole and extend to the periphery with increasing trauma severity. Our data do not suggest any morphological characteristics in the immature retinal vasculature that could suggest an increased vulnerability in the posterior pole compared to the equator. However, the clinical finding that posterior pole RH is far more common could be a function of many other factors that influence the location or type of RH, such as the applied loading directions in accidental and abusive head trauma, rather than the microstructural features. These loading directions and magnitudes will be affected by the infant head and neck anatomical features and control. There have been no known studies investigating the directionality of head loading on the severity of RH in infants; however, sagittal head rotations may result in more direct loading to the posterior pole than the equator. This would result in increased risk of RH in the posterior pole if vitreoretinal traction is the mechanism of RH. Any contributions of increased pressurization to the risk of RH would not be affected by loading direction. More research is needed to elucidate the role of these mechanisms and the distribution of loading to the retina in accidental and abusive trauma.

## Conclusions

We investigated morphological characteristics in the infant retinal vasculature that may or may not make it more susceptible to hemorrhage during traumatic loading events. We selected key characteristics influential in vessel network mechanics for our study and, through confocal microscopy, image processing, and statistical analysis, determined the prevalence of each of the characteristics as a function of region, depth, and age. Vessel lengths were shorter and more highly branched in preterm retinas compared to adult specimens. These characteristics suggest increased potential for strain and stress failure, respectively, in infant vessels compared to adults, as well as a greater number of stress concentrations at the branch points. Further, decreased vessel diameter and increased tortuosity with depth, regardless of age, reflect a general increased risk of RH in deeper layers of the retina. However, these two characteristics may appear different in vivo in a state of physiological pressurization. The morphological features captured in this study lay the foundation to biomechanically explore the mechanics of RH in infants and identify vulnerabilities that may help explain patterns of RH in infants.

## *Acknowledgments*

The authors thank Tara Mleynek for assistance in developing the staining protocol and Chris Rodesch at the University of Utah Core Cell Imaging Facility for his assistance with imaging.

Supported in part by National Institutes of Health Grant No. R21EY025813. Imaging was performed at the Fluorescence Microscopy Core Facility, a part of the Health Sciences Cores at the University of Utah. Microscopy equipment was obtained using National Center for Research Resources Shared Equipment Grant No. 1S10RR024761-01.

Disclosure: **M.P. Byrne,** None; **K.R. McMillan**, None; **B. Coats**, None

## *References*

1. Binenbaum G, Mirza-George N, Christian CW, Forbes BJ. Odds of abuse associated with retinal hemorrhages in children suspected of child abuse. *J AAPOS*. 2009;13:268–272.
2. Duhaime AC, Christian CW, Rorke LB, Zimmerman RA. Nonaccidental head injury in infants–the "shaken-baby syndrome." *N Engl J Med*. 1998;338:1822–1829.
3. Rao N, Smith RE, Choi JH, Xu XH, Kornblum RN. Autopsy findings in the eyes of fourteen fatally abused children. *Forensic Sci Int*. 1988;39:293–299.
4. Harcourt B, Hopkins D. Ophthalmic manifestations of the battered-baby syndrome. *Br Med J*. 1971;3:398–401.
5. Morad Y, Kim YM, Armstrong DC, Huyer D, Mian M, Levin AV. Correlation between retinal abnormalities and intracranial abnormalities in the shaken baby syndrome. *Am J Ophthalmol*. 2002;134:354–359.
6. Martinez-Perez ME, Hughes AD, Stanton AV, et al. Retinal vascular tree morphology: a semi-automatic quantification. *IEEE Trans Biomed Eng*. 2002;49:912–917.
7. Hellstrom A, Svensson E. Optic disc size and retinal vessel characteristics in healthy children. *Acta Ophthalmol Scand*. 1998;76:260–267.
8. Stromland K, Hellstrom A, Gustavsson T. Morphometry of the optic nerve and retinal vessels in children by computer-assisted image analysis of fundus photographs. *Graefes Arch Clin Exp Ophthalmol*. 1995;233:150–153.
9. Kromer R, Buhmann C, Hidding U, et al. Evaluation of retinal vessel morphology in patients with Parkinson's disease using optical coherence tomography. *PLoS One*. 2016;11:e0161136.
10. Witt N, Wong TY, Hughes AD, et al. Abnormalities of retinal microvascular structure and risk of mortality from ischemic heart disease and stroke. *Hypertension*. 2006;47:975–981.
11. Binenbaum G, Chen W, Huang J, Ying GS, Forbes BJ. The natural history of retinal hemorrhage in pediatric head trauma. *J AAPOS*. 2016;20:131–135.
12. Maguire SA, Watts PO, Shaw AD, et al. Retinal haemorrhages and related findings in abusive and non-abusive head trauma: a systematic review. *Eye (Lond)*. 2013;27:28–36.

13. Park JJ, Soetikno BT, Fawzi AA. Characterization of the middle capillary plexus using optical coherence tomography angiography in healthy and diabetic eyes. *Retina*. 2016;36:2039–2050.
14. Tan PE, Yu PK, Balaratnasingam C, et al. Quantitative confocal imaging of the retinal microvasculature in the human retina. *Invest Ophthalmol Vis Sci*. 2012;53:5728–5736.
15. Chan G, Balaratnasingam C, Yu PK, et al. Quantitative morphometry of perifoveal capillary networks in the human retina. *Invest Ophthalmol Vis Sci*. 2012;53:5502–5514.
16. Colter J, Williams A, Moran P, Coats B. Age-related changes in dynamic moduli of ovine vitreous. *J Mech Behav Biomed Mater*. 2015;41:315–324.
17. Prange MT, Margulies SS. Regional, directional, and age-dependent properties of the brain undergoing large deformation. *J Biomech Eng*. 2002;124:244–252.
18. Creveling CJ, Colter J, Coats B. Changes in vitreoretinal adhesion with age and region in human and sheep eyes. *Front Bioeng Biotechnol*. 2018;6:153.
19. Dobbing J. The later growth of the brain and its vulnerability. *Pediatrics*. 1974;53:2–6.
20. Prince J, Diesem C, Eglitis I, Ruskell G. *Anatomy and histology of the eye and orbit in domestic animals*. Springfield, IL: Charles C Thomas; 1960.
21. Saffioti J. *Characterization of pediatric ocular material properties for implementation in finite element modeling*. Salt Lake City, UT: Department of Mechanical Engineering, University of Utah; 2014.
22. Nowak-Sliwinska P, Weiss A, Sickenberg M, Griffioen AW, van den Bergh H. The role of photodynamic therapy in non-malignant and malignant eye disorders. *J Anal Bioanal Tech*. 2013;S1:1–25.
23. McMillan K, Byrne M, Coats B. *VascularMorphology*. Available at: https://github.com/UtahHeadTrauma/VascularMorphology . Accessed January 21, 2020.
24. Anand-Apte B, Hollyfield HJG. Developmental anatomy of the retinal and choroidal vasculature. In: Dartt DA, Besharse JC, Dana R , eds. *Encyclopedia of the eye*. Oxford, UK: Academic Press; 2010:9–15.
25. Monson KL, Converse MI, Manley GT. Cerebral blood vessel damage in traumatic brain injury. *Clin Biomech (Bristol, Avon)*. 2019;64:98–113.
26. Han HC. Twisted blood vessels: symptoms, etiology and biomechanical mechanisms. *J Vasc Res*. 2012;49:185–197.
27. Kylstra JA, Wierzbicki T, Wolbarsht ML, Landers MB, Stefansson E. The relationship between retinal vessel tortuosity, diameter, and transmural pressure. *Graefes Arch Clin Exp Ophthalmol*. 1986;224:477–480.
28. Martinez R, Fierro CA, Shireman PK, Han HC. Mechanical buckling of veins under internal pressure. *Ann Biomed Eng*. 2010;38:1345–1353.
29. Monson KL, Barbaro N, Manley G. Cerebrovascular injury in head trauma - susceptibility of branch points. *J Neurotrauma*. 2008;25:864.
30. Fenton TR, Gibson WG, Taylor JR. Stress analysis of vasoconstriction at arterial branch sites. *J Biomech*. 1986;19:501–509.
31. Thubrikar MJ, Roskelley SK, Eppink RT. Study of stress concentration in the walls of the bovine coronary arterial branch. *J Biomech*. 1990;23:15–26.
32. Mitchell P, Jakubowski J. Failure testing cerebral arteries: are branch points weaker than unbranched vessels? *Br J Neurosurg*. 2002;16:578–582.

Investigative Ophthalmology & Visual Science